# Spatial evolution of frictional heating and the predicted thermospheric wind effects in the vicinity of an auroral arc measured with the Sondrestrom incoherent-scatter radar and the Reimei satellite

S. Oyama,[1,2] T. T. Tsuda,[1] T. Sakanoi,[3] Y. Obuchi,[3,4] K. Asamura,[5] M. Hirahara,[6] A. Yamazaki,[5] Y. Kasaba,[7] R. Fujii,[1] S. Nozawa,[1] and B. J. Watkins[2]

[1]   Simultaneous observation with the Sondrestrom incoherent-scatter (IS) radar and the Reimei satellite was conducted on 3 October 2007. The objective was to measure horizontal patterns of the ionospheric structure in the vicinity of an auroral arc. The IS radar was scanned azimuthally with a fixed elevation angle, and the satellite narrow-view camera (557.7 nm) was directed downward taking pictures every 0.12 s. A stationary auroral arc was captured at 05:17 UT (02:54 MLT) with both instruments simultaneously. Gross ionospheric features measured with the IS radar around the arc were in good agreement with the expected magnetosphere-ionosphere current system. Of particular interest was the horizontal pattern in the ion speed and temperature in the $F$ region. The ion speed within the arc was close to zero; by contrast the larger ion speed ($350-400$ m s$^{-1}$) on the poleward side was parallel to the arc and almost no horizontal shear within about 20 km width perpendicular to the arc. This area was separated into two parts by the ion temperature: one was associated with clear enhancements in excess of 1200 K, and another was with more moderate enhancements (less than $\sim$1000 K). The widths of the two areas were approximately 10 km each. The horizontal shear seen in the ion temperature suggested the presence of a narrow thermospheric wind shear of about 10 km width. This paper suggests that the possible cause for the thermospheric wind shear was ion drag associated with localized soft particle precipitation or $F$-region ionization.

## 1. Introduction

[2]   At high latitudes, electromagnetic and particle energy is transferred from the magnetosphere to the ionosphere and the thermosphere. The polar ionosphere and thermosphere act as an energy and particle sink, where the energy is transformed into both heated and accelerated plasmas and neutral particles. The former and latter process can be regarded as energy transformation to thermal and mechanical energy, respectively. These processes cause, for example, accelerated winds and atmospheric gravity waves in the polar thermosphere with various spatiotemporal scales [*Francis*, 1974; *Kato et al.*, 1977; *Hunsucker*, 1982; *Fuller-Rowell*, 1984; *Hajkowicz*, 1991; *Millward et al.*, 1993; *Fujiwara et al.*, 1996; *Fuller-Rowell et al.*, 1996; *Hocke and Schlegel*, 1996; *Richards and Wilkinson*, 1998; *Smith*, 2000; *Aruliah and Griffin*, 2001; *Ishii et al.*, 2001, 2004; *Oyama et al.*, 2001, 2008; *Tsugawa et al.*, 2003, 2004; *Aruliah et al.*, 2005]. The majority of these thermospheric wind variations are regarded as the passive features to the energy input from the magnetosphere. However, the thermospheric winds can also play an active role in the coupled Magnetosphere-Ionosphere-Thermosphere (MIT) system [*Lu et al.*, 1995; *Fujii et al.*, 1998, 1999; *Thayer*, 1998, 2000]. *Lu et al.* [1995] revealed that the neutral winds had approximately a 28% negative effect on Joule heating on the global average for an event; but greater effects can be locally appeared [*Cierpka et al.*, 2000].

[3]   The ionospheric current system adjacent to the auroral arc has been studied for four decades using data taken with satellites [*Maggs and Davis*, 1968; *Weimer et al.*, 1985;

[1]Solar-Terrestrial Environment Laboratory, Nagoya University, Nagoya, Japan.

[2]Geophysical Institute, University of Alaska Fairbanks, Alaska, USA.

[3]Planetary Plasma and Atmospheric Research Center, Graduate School of Science, Tohoku University, Sendai, Japan.

[4]Now at Genesia Corporation, Tokyo, Japan.

[5]Department of Space Plasma Physics, Japan Aerospace Exploration Agency, Institute of Space and Astronautical Science, Kanagawa, Japan.

[6]Department of Earth and Planetary Science, Graduate School of Science, University of Tokyo, Tokyo, Japan.

[7]Planetary Atmosphere Physics Laboratory, Graduate School of Science, Tohoku University, Sendai, Japan.

*Marklund et al.*, 1994, 1997, 2001, 2004, 2007; *Karlsson and Marklund*, 1996; *Gustavsson et al.*, 1997; *Mozer and Kletzing*, 1998; *Ergun et al.*, 1998, 2000, 2002; *Knudsen et al.*, 2001; *Andersson et al.*, 2002; *Lynch et al.*, 2002; *Johansson et al.*, 2004, 2007; *Figueriredo et al.*, 2005; *Hwang et al.*, 2006a, 2006b], rockets [*Potter*, 1970; *Kintner et al.*, 1974; *Carlson and Kelley*, 1977; *Evans et al.*, 1977; *Cahill et al.*, 1980; *Thiele et al.*, 1981; *Marklund et al.*, 1982, 1983; *Ziesolleck et al.*, 1983], and radars [*de la Beaujardiere et al.*, 1977, 1981, 1982; *Stiles et al.*, 1980; *Villain et al.*, 1987, 1990; *Milan and Lester*, 2001; *Milan et al.*, 2001, 2002, 2003; *Moen et al.*, 2008]. In the upward field-aligned current (FAC) region, energetic electron precipitation causes auroras and ionization mainly at heights that depend on the precipitating particle energy. The ionospheric electron density at the outside of the auroral arc is frequently lower than the surrounding background level because of evacuation of plasma to the magnetosphere in association with the downward FAC [*Marklund et al.*, 1994, 2004]. The depletion region may appear at the magnetic poleward or equatorward side of the arc depending on the relative position of the observed ionosphere in relation to the ionospheric convection cell [*Milan et al.*, 2002, and references therein]. In the ionospheric depletion region, the electric field perpendicular to the arc usually has obvious enhancements, which bring ions in the depletion region within the arc to maintain electrical neutrality. That ion motion perpendicular to the arc is equivalent to the Pedersen current, which permits the current closure between the magnetosphere and the ionosphere. The electric field accelerates ions through the background neutral particles. That relative speed between ions and neutrals then results in ion-temperature enhancements, in particular in the *F* region, through the frictional heating process as described by the ion-energy equation [e.g., *St.-Maurice and Hanson*, 1982; *Killeen and Roble*, 1988, and references therein].

[4] Ionospheric ions accelerated by intense electric field also drag neutral particles by collisions. While the pressure gradient between the sunlit and the dark hemispheres create the fundamental pattern of polar thermospheric wind at *F*-region heights, ion drag is also an important additional force for the wind at high latitudes [*Fuller-Rowell and Rees*, 1980; *Sica et al.*, 1986; *Killeen and Roble*, 1988; *Aruliah et al.*, 1991a, 1991b; *Crickmore*, 1994; *Niciejewski et al.*, 1996]. Some observations suggest that the thermospheric winds at *F*-region heights can follow sudden changes in the ionospheric convection pattern because of IMF (Interplanetary Magnetic Field) variations but with some delays [*Conde et al.*, 2001]. The thermospheric winds can only respond to a change in ion motions on a timescale of 10 min or greater at *F*-region heights [*Baron and Wand*, 1983; *Killeen et al.*, 1984; *Kosch et al.*, 2001]; but it is dependent on the plasma density. If there is no relative speed between ions and neutral particles, the ion temperature cannot be increased according to the frictional-heating theory.

[5] The mesoscale structures in the high-latitude ion velocity and thermospheric wind have been reported in several publications [*Codrescu et al.*, 2000; *Aruliah and Griffin*, 2001; *Matsuo et al.*, 2002, 2003, 2005; *Shepherd et al.*, 2003; *Aruliah et al.*, 2005; *Matsuo and Richmond*, 2008]. Such structures tend to be localized in space and appeared for a short time. Ionospheric fine structures may affect the global wind dynamics in the thermosphere by dissipating more energy than predicted when short-term fluctuations in ion motion are considered. In practice, even after averaging abundant data sets from observations, we can find some notable differences of the thermospheric wind from results of empirical and global circulation models (GCM) [*Aruliah and Griffin*, 2001]. Both generation mechanisms and effects of the mesoscale ionospheric/thermospheric structures remain fundamental questions in this field.

[6] We have conducted a simultaneous observation with the Sondrestrom incoherent-scatter (IS) radar (67°N, 309°E, 73° magnetic latitude) in Greenland, Denmark and the Reimei satellite [*H. Saito et al.*, 2001; *Asamura et al.*, 2003; *Sakanoi et al.*, 2003] on 3 October 2007. The scientific objective of this experiment is to capture the ionospheric image around the auroral arc with a good spatial resolution of a few kilometers in the *F* region. The magnetospheric and ionospheric condition during the observation will be mentioned in section 2. The details of the observation configuration will be presented in section 3. section 4 will show the observation results. The majority of the results regarding the ionospheric current system associated with the auroral arc is in fairly good agreement with the theory proposed by previous studies. However, an important signature has been found in the IS radar data, which will be helpful to improve our understanding of the coupled MIT system. This finding will be discussed in section 5. The summary and conclusions will be presented in section 6.

## 2. Magnetosphere and Ionosphere During the Observation

[7] Variations in the polar ionosphere are dependent on solar-wind parameters such as the solar-wind speed and IMF. These parameters should be addressed to capture the gross features in the magnetosphere and the ionosphere. The solar-wind speed measured with the ACE spacecraft from 03:30 to 04:30 UT is approximately 460 km s$^{-1}$, which suggests that it takes about 50 min for the solar-wind plasma to reach the terrestrial magnetosphere from the ACE position. Since the event interested in this paper has appeared at 05:17 UT, here we focus on the solar-wind parameters taken around 04:27 UT. While IMF $B_x$ and the total magnetic field remained negative and about 6 nT, respectively, from 04:00 to 05:00 UT, IMF $B_y$ jumped from ∼0 to ∼3 nT at 04:13 UT. After that IMF $B_y$ did not have notable variations by 04:43 UT. For that 30 min (from 04:13 to 04:43 UT), IMF $B_z$ gradually changed from negative to positive, crossing 0 nT at 04:27 UT. The particle density and the dynamic pressure from 04:00 to 05:00 UT remained almost constant at about 10 cm$^{-3}$ and 3 nPa, respectively. Kp index from 3 to 6 UT was 4-. F10.7 index (Ottawa 10.7-cm solar radio flux adjusted to 1 AU in 10$^{-22}$ W/m$^2$/Hz) was 67.3 or low solar activity.

[8] Figure 1 shows the ionospheric convection pattern deduced from the SuperDARN radar every 6 min (but 2-min data acquisition) from 05:04 to 05:24 UT. Greenland is colored in pink for reference. The convection map shown in Figure 1c is made from data acquired during simultaneous observations between the Sondrestrom IS radar and the Reimei satellite. At the upper right corner of Figures 1a–1d,
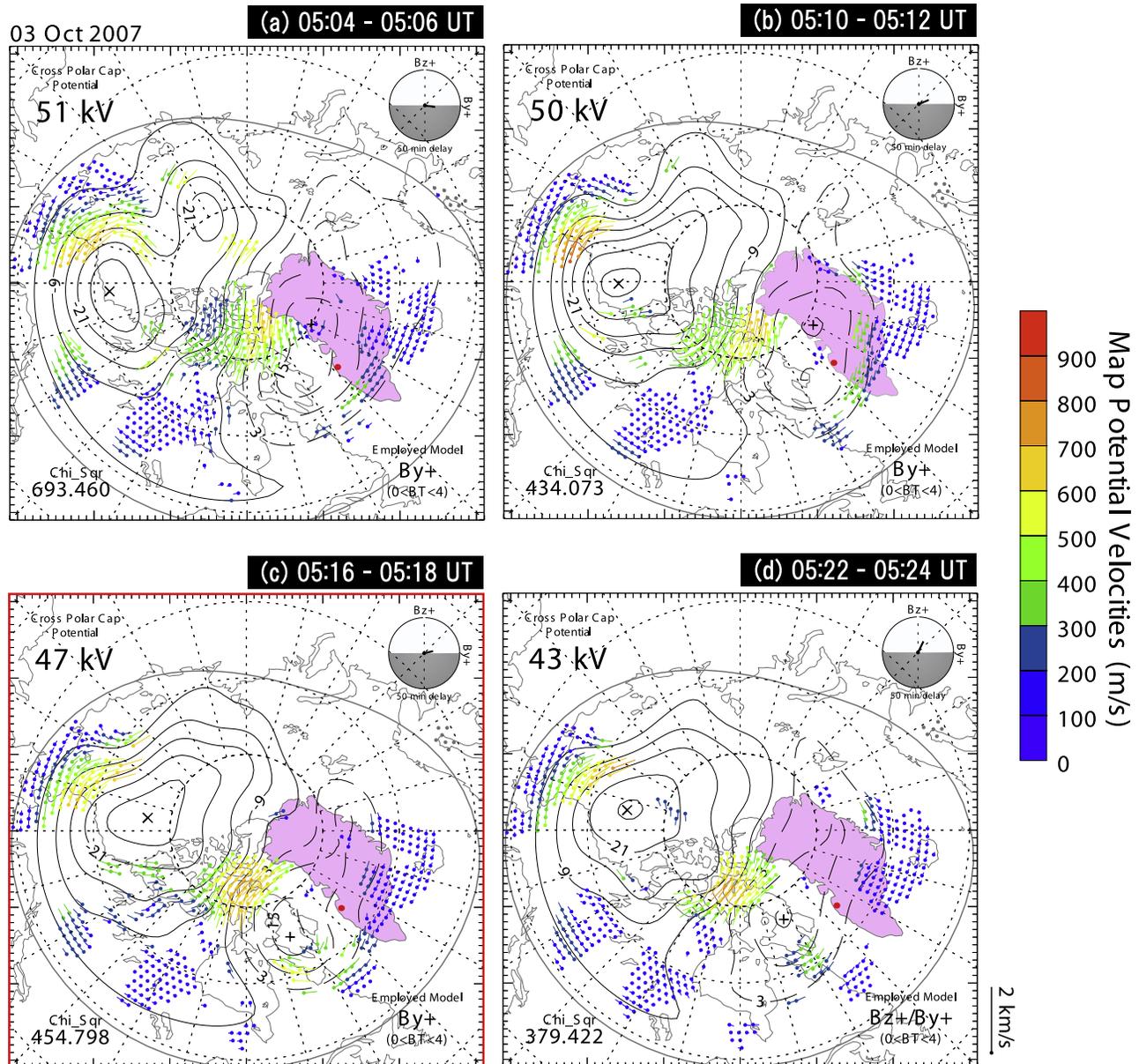
**Figure 1.** Ionospheric convection pattern estimated from data taken with the SuperDARN radars at (a) 05:04–05:06 UT, (b) 05:10–05:12 UT, (c) 05:16–05:18 UT, and (d) 05:22–05:24 UT on 3 October 2007. The IMF direction at each time is illustrated at the upper right corner of each Figures 1a–1d but with 50-min delay from the ACE observation by taking into account the solar-wind speed. The cross polar cap potential at each time is shown in the upper left corner of Figures 1a–1d. Greenland is in pink. The solid red circle is plotted at the Sondrestrom IS radar site. The ion-speed scale is shown at the lower right corner and also in color as shown at the right. The convection pattern of Figure 1c in the red square was taken at the simultaneous observation between the Sondrestrom IS radar and the Reimei satellite.

the IMF direction is illustrated but with 50 min delay from the ACE observation. The gross features are in good agreement with a statistical pattern derived by *Ruohoniemi and Greenwald* [2005] for individual IMF $B_y$ and $B_z$ conditions. While IMF $B_z$ component with 50 min delay turns from negative to positive around these times, the convection patterns do not show notable differences among them. It is worthy of mentioning that the simultaneous observation area is in the morning convection cell. This suggests that the

dominant component of the background electric field is southward in the observation region.

## 3. Instruments

[9] The Sondrestrom IS radar was operated from 04:17:59 to 05:50:51 UT (LT = UT − 3 hours; MLT = UT − 2 hours and 23 min) on 3 October 2007. The radar antenna azimuthally scanned the ionosphere with a fixed elevation angle of 30°. The full width of the azimuth scan

REIMEI MAC2 (557.7 nm)
03-Oct-2007 05:16:44 to 05:17:16 UT
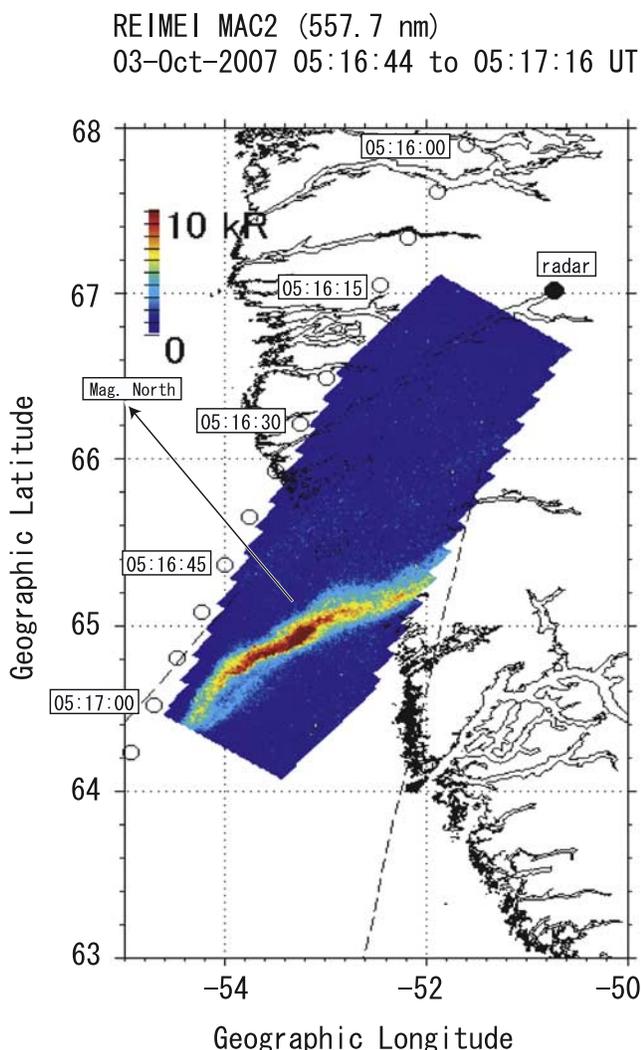


**Figure 2.** Integrated images taken with the aurora camera (MAC; 557.7 nm) on board the Reimei satellite every 2.4 s from 05:16:43.996 to 05:17:16.059 UT on 3 October 2007. The images are mapped on the geographic coordinate assuming the emission layer of 120 km. The coast line around the southwest of Greenland is drawn with a solid curve. The color scale is presented at the upper left corner. The solid circle is plotted at the Sondrestrom IS radar site. The edges of the field-of-view of the IS radar for one sequence are illustrated with the long dashed lines. The open circles represent the foot point of the magnetic field line at 120 km. The direction of magnetic north is illustrated by a black arrow.

was 24° (between 190.5° and 214.5° clockwise from geographic north), which was designed to cover the field-of-view (FOV) of the Reimei satellite camera. The scan speed was 0.1° per second. The data were integrated for 5 s or 0.5° width in azimuth. One sequence of the scan, which was 240 s, contained 48 bins in azimuth. The width of the bin was approximately equal to 2 km in the $F$ region. The pulse length was 320 $\mu$s, and the ACF (autocorrelation function) sampling was separated by 21 km range. The ionospheric parameters such as the electron density, the ion/electron temperature, and line-of-sight (LOS) ion speed

were derived from the IS spectrum obtained from individual ACF. This means that the ionospheric data were derived every 11 km height (= $21 \times \sin 30°$) and 18 km horizontally (= $21 \times \cos 30°$) along the radar beam. The ionospheric parameters in the lower $E$ region where the scale height is less than 11 km might introduce some ambiguity compared to the $F$ region. Data in the $E$ region may not be sufficient for quantitative studies; but is still available in a qualitative manner. Data in the $F$ region (above ~150 km) will be used for quantitative studies.

[10] The Reimei satellite was launched on 23 August 2005 into sun-synchronous orbit with an altitude between 610 and 670 km and inclination of 97.8°. Five scientific instruments were carried: a three channel monochromatic auroral imaging CCD camera (MAC) [*Sakanoi et al.*, 2003], top-hat-type auroral electron and ion-energy spectrum analyzers (ESA and ISA, respectively) [*Asamura et al.*, 2003], current probes (CRM), and magnetic field sensors (GAS). In this paper data taken with MAC, ESA, and ISA are used. The MAC three emission lines were $N_2^+$ first negative band (427.8 nm), OI (557.7 nm), and $N_2$ first positive band (670.0 nm). During the experiment on 3 October 2007, the camera of 427.8 nm was off to save the electric power. While the other two channels were operated, only data taken with the 557.7-nm camera are presented in this paper because data taken with the 670.0-nm camera are contaminated by strong reflection of the aurora from the tropospheric clouds or the surface of earth. The MAC FOV (7.6°; $79 \times 79$ km$^2$ at 120 km altitude) was directed almost downward (to the earth) during the experiment to monitor horizontal distributions of the auroral emission. The time resolution of image data was 120 ms. ESA and ISA obtained the energy spectrum of electrons and ions in the energy range of 12–12,000 eV and 10–12,000 eV, respectively, with 16 or 32 energy steps. The time resolution was 20 ms (40 ms) for the 16 (32) energy-step case. The FOV at individual directions was 4°, and it was directed within 300° in polar angle direction. While FOV of ESA/ISA was able to be directed within FOV of MAC by controlling the satellite position, the FOV of ESA/ISA was not controlled for the experiment on 3 October 2007 because the first priority of the experiment was to direct the camera downward. However, the foot point of the ESA/ISA FOV was unexpectedly close to MAC FOV as shown in the next section. The Reimei satellite flew directly above the Sondrestrom radar site (maximum elevation angle of 89.8°) at 05:16:03 UT at 645.75 km height.

## 4. Results

[11] Figure 2 shows the auroral arc taken with the Reimei MAC (wavelength = 557.7 nm) mapping on the 120-km height layer. The satellite moves from northeast to southwest at approximately 7.5 km s$^{-1}$ at 645 km height. Thus the area covered with the MAC is shifted by 0.9 km (= 7.5 km s$^{-1}$ × 0.12 s) every snapshot along the satellite path. To make Figure 2, 14 images are overlaid on the map by selecting an image every 20 snapshots or 2.4 s. The radar site is marked by the solid circle. The edge of FOV of the dwelling radar beam is illustrated by dashed line as reference. The open circles are the foot points of the magnetic field line crossing the satellite. They are marked
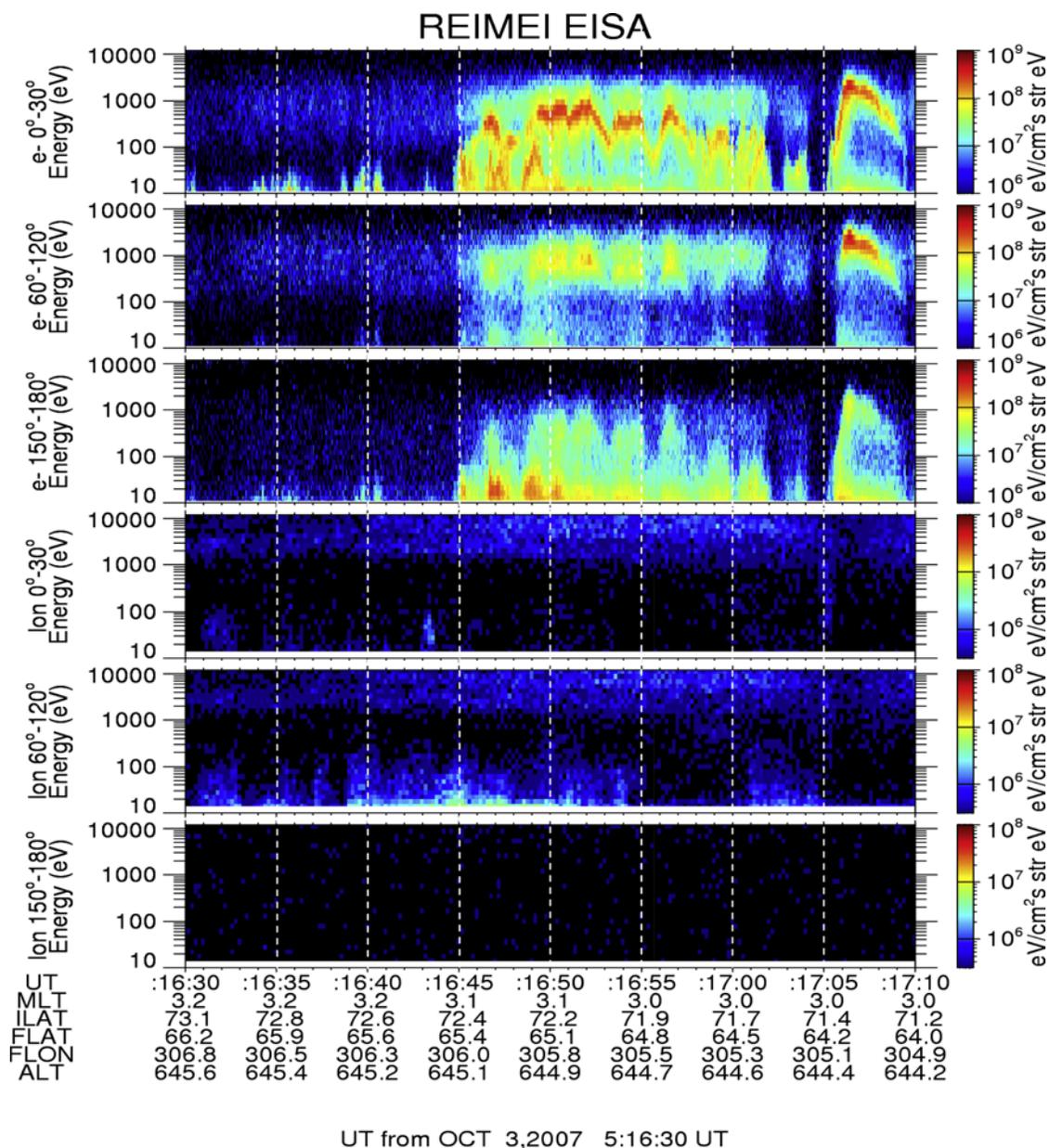
**Figure 3.** Electron and ion-energy spectra measured with the Reimei ESA/ISA between 05:16:30 and 05:17:10 UT on 3 October 2007. Vertical white dashed lines are drawn every 5 s for reference.

every 5 s, and several time stamps are illustrated every 15 s in the square. The foot points are gradually approached toward the Reimei MAC FOV because of inclination/declination of the local magnetic field line. That is not caused by the rotation of the satellite itself, and the satellite maintains a downward looking direction without rotation. Images taken during the second half of this time interval capture an auroral arc extending along almost magnetic zonal direction. This arc is appeared almost in the center of FOV without notable motions at least for this time interval. The almost stationary auroral structure adjacent to the radar is most advantageous for data comparisons.

[12] The particle measurements have been conducted with ESA/ISA together with MAC. While the foot points are slightly deviated from the camera FOV toward the magnetic poleward (see Figure 2), ESA and ISA provide data to supplement the horizontal pattern of particle precipitation around the auroral arc. Figure 3 shows the electron and ion-energy spectra for 40 s from 05:16:30 to 05:17:10 UT on 03 October 2007. White dashed lines are marked every 5 s as a reference. From 05:16:30 to 05:16:45 UT, when the foot points are located far from the arc, the instruments do not detect anything notable. From 05:16:45 to 05:17:02 UT, when the foot points are mainly located at the poleward side of the arc, several inverted-V structures are seen in the downward ($0°-30°$; top) electron spectra but the peak energies for individual inverted-V structures are lower than 1 keV. Since the stopping height for precipitating electrons of 1 keV is about 150 km, the ionosphere at the poleward side of the arc must be ionized above 150 km but not down to the $E$ region. This result is consistent with weak visible aurora at 557.7 nm, which generally
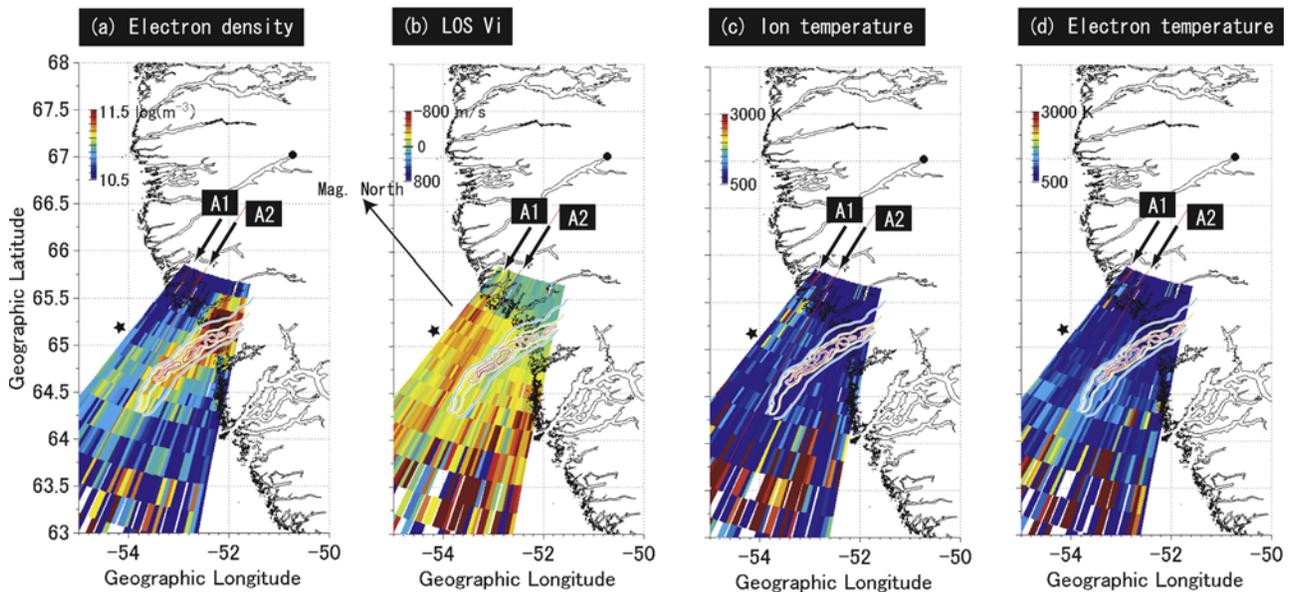
**Figure 4.** Horizontal patterns of (a) the electron density, (b) the line-of-sight ion speed, (c) the ion temperature, and (d) the electron temperature measured with the Sondrestrom IS radar from 05:14:34 to 05:18:35 UT on 3 October 2007. Note that the negative (positive) or warm (cold) color in the ion speed is toward (away from) the radar. The direction of magnetic north is illustrated by a black arrow in Figure 4b. The range gate that gives data used in Figure 5 is marked by a star. The contour plot of the auroral arc shown in Figure 2 is overlaid on Figures 4a–4d but arranging its shape taking into account the magnetic field declination and inclination. The solid red line represents the main radar beam direction while taking the aurora images. A1 and A2 illustrate areas 1 and 2, respectively (see the text for details). The radar site is marked with a solid circle.

has a peak below 150 km, at the poleward side of the arc. It should be stated that diffuse aurora with the emission intensity of about 2 kR can be identified in that area by changing the color scale (not shown here). From 05:17:05 to 05:17:09 UT, an inverted-V structure with higher peak energy is seen in the spectra of downward electrons. The peak energy is about 3 keV, which corresponds to the stopping height of ~120 km. The arc appears to be more extended toward magnetic westward though it is outside of the MAC images, and the foot point gradually approaches to the arc with time because of inclination/declination of the magnetic field line as mentioned before. These experimental evidences are good reasons to assume that the foot points for the 4 s (from 05:17:05 to 05:17:09 UT) are located inside the arc. One may think that the arc can be identified in the electron density measured with the IS radar. However, the IS radar data is not available for that purpose because of the $F$-region data above 200 km in the area where the inverted-V structure was measured. The ion-energy spectra do not show notable enhancements for the time shown in the Figure 3.

[13] Figure 4 shows the ionospheric parameters of (a) electron density, (b) LOS ion speed, (c) ion temperature, and (d) electron temperature measured with the Sondrestrom IS radar (located at the solid circle) for one sequence from 05:14:34 to 05:18:35 UT on 3 October 2007. Height at the nearest range gate from the radar is 96.3 km, then increasing by approximately 11 km with each range gate. For example, height at the 6th range gate is 151.59 km. Negative (positive) values of the LOS ion speed show the ion motion toward (away from) the radar. Note that negative (positive) values are illustrated in warm (cold) colors, which might be different from the general manner. The red solid line presents the radar beam direction when the satellite has flown over this area. The contour plot of auroral arc shown in Figure 2 is overlaid on the IS radar data. One may see that the auroral-arc position in Figure 4 is slightly different from that in Figure 2. This is because the auroral arc in Figure 4 is mapped on heights of radar observations taking into account inclination/declination of the local magnetic field line at each data point. This modification works well because electron-density enhancements are exactly overlapped on the auroral arc as shown in Figure 4a.

[14] The electron density shows large enhancements in the auroral arc. This is a typical response of the ionosphere to auroral particle precipitation. The electron density at the magnetic poleward side of the arc, marked by A1, shows obvious depletions (below $10^{11}$ $m^{-3}$) in both $E$ and $F$ regions; but the electron density beyond the 7th gate show moderate enhancements. Between the arc and A1, the electron density shows weak but clear enhancements in the $F$ region (from 64.5°N to 65°N) but depletions in the $E$ region (from 65.3°N to 65.8°N). We denote this area as A2 in this paper. Electron-density depressions in the vicinity of

the auroral arc have been measured with satellites, rockets, and IS radars [*de la Beaujardiere et al.*, 1977; *Evans et al.*, 1977; *Cahill et al.*, 1980; *Theile et al.*, 1981; *Marklund et al.*, 1982, 1983, 1997, 2001; *Gustavsson et al.*, 1997; *Freja Special Issue*, 1998; *Karlsson and Marklund*, 1998; *Hultqvist*, 2002]. It is considered that the up-going electrons originated in the ionosphere or the downward field-aligned current cause the electron-density depression. The upward field-aligned currents present in the auroral arc in association with the down-going accelerated electrons or auroral particle precipitation. The current continuity is a balance between the field-aligned current density integrated along the geomagnetic field line from the base to the top of the ionosphere and the divergence of the current density perpendicular to the geomagnetic field line. To sustain the current continuity system, the ionospheric electric field perpendicular to the auroral arc is enhanced to increase the Pedersen current. Since the major force to control the horizontal ion motion in the $F$ region is $\mathbf{E} \times \mathbf{B}$, the $F$-region ion speed in the downward field-aligned current region should be accelerated along the auroral arc. This acceleration can be seen in A1 and A2 of Figure 4b, which shows horizontal patterns of the LOS ion speed. The ion speeds in both A1 and A2 are almost identical at about 350–400 m s$^{-1}$. Since the ion speed measured with the Sondrestrom IS radar for this event is only the LOS component, the perpendicular component to the LOS cannot be estimated. However, the ion velocity vector estimated with the SuperDARN radars over this area from 05:14 to 05:18 UT is almost parallel to the IS radar LOS. Thus it is considered that the ion speeds shown in Figure 4b are close enough to the total velocity. The magnitude of the electric field can be estimated as approximately 18–20 mV m$^{-1}$.

[15] Figure 4c shows the horizontal pattern of the ion temperature. The ion temperature in A1 shows clear enhancements; but enhancements in A2 appear to be more moderate than A1. The electron temperature, shown in Figure 4d, also shows enhancements at $E$-region height in A1 but not in A2. While the $E$-region data should not be used in a quantitative manner as mentioned in section 3, the enhancements may be caused by the Farley-Buneman instability, which can be caused by electric fields larger than 20–30 mV m$^{-1}$ [*Schlegel and St.-Maurice*, 1981; *Davies and Robinson*, 1997; *Saito et al.*, 2001]. This may imply that the electric field in A1 is larger than the threshold but smaller in A2. However, differences in the electric-field magnitude between the two areas must not be large according to the horizontal pattern of the ion speed. The difference may be less than a few mV m$^{-1}$.

[16] The ionosphere at the magnetic equatorward side of the arc may also be characterized in a similar manner as the poleward side; but data look noisier because of larger range. Thus this paper focuses on the poleward side. The similar signature of the ionospheric parameters can be identified in the FOV of the IS radar from 05:06 to 05:22 UT (not shown here). It is thus considered that the flow channel has appeared at least for 16 min in the observation area.

[17] While Figure 4 gives us the ideal horizontal image of the ionospheric current system associated with the auroral arc, Figure 5 may be better suited for a quantitative comparison among ionospheric parameters. From top to bottom, data of (a) electron density, (b) LOS ion speed, (c) ion temperature, and (d) electron temperature taken at 151.59 km altitude are shown. The two areas, A1 and A2, are hatched in dark and moderate gray, respectively. The auroral arc appeared from $-53.2°$ to $-52.15°$ longitude (hatched in light gray). While this Figure 5 shows a one-dimensional pattern at one height, signatures mentioned in Figure 4 are well captured: (1) high electron density, small LOS ion speed, low ion temperature in the auroral arc, (2) low electron density, large LOS ion speed, strong enhancements in the ion temperature in A1, and (3) moderate electron density, large LOS ion speed, weaker enhancements in the ion temperature in A2. The electron temperature in A1 does not show enhancements because the data pertain to the $F$-region altitude.

[18] Figure 4 suggests that the electric fields in both A1 and A2 are approximately 20 mV m$^{-1}$. However, one may query why the ion temperature in A2 has smaller values than A1 when taking into account the frictional heating process. To understand this issue, we need to consider effects of the neutral wind that will be discussed in the next section.

## 5. Discussion

[19] As mentioned in section 1, spatiotemporal relationships between the electric field and the potential structure in the magnetosphere have been studied by many researchers using satellite data (up to ~2000 km height). For example, of particular interest in the recent findings is very intense (>100 mV m$^{-1}$) and narrow (~1 km) structures of the electric field appeared in the vicinity of the energetic electron precipitation [*Marklund et al.*, 1994, 1997, 2001, 2004; *Ergun et al.*, 1998, 2000, 2002; *Andersson et al.*, 2002; *Lynch et al.*, 2002; *Johansson et al.*, 2004; *Figueiredo et al.*, 2005]. Such electric fields are characterized by the divergent structure. Since the divergent electric field is frequently observed in association with the downward current or up-going electrons from the ionosphere, it is suggested that the intense divergent electric field is related to the enhanced Pedersen current in the current closure system. Ionospheric ions move from the downward current region to the upward current region in association with the Pedersen current. This motion is perpendicular to the magnetic field line and also to the auroral arc. Since the ionospheric frictional heating process coincides with the Pedersen current enhancement, the $F$-region ion temperature is promptly increased in response to applied electric fields from the magnetosphere. Actually, the $F$-region ion temperature measured with IS radar shows fairly good correlation with electric-field variations [*Fujii et al.*, 2002]; but there are some exceptions, which may be caused by an active role of the thermospheric wind. The hypothesis proposed here to explain the ion-temperature difference between A1 and A2 is that the relative speed between ions and neutral particles is larger in A1 than A2. This means that the neutral wind has horizontal shears between the two areas. Figure 5 shows that increases in the ion temperature in A2 are smaller than those in A1 though the ion speeds are in almost same level between the two areas. While there is no observed data of the neutral wind for this event, it is worthy of discussing possible effects of the horizontal shears of the horizontal
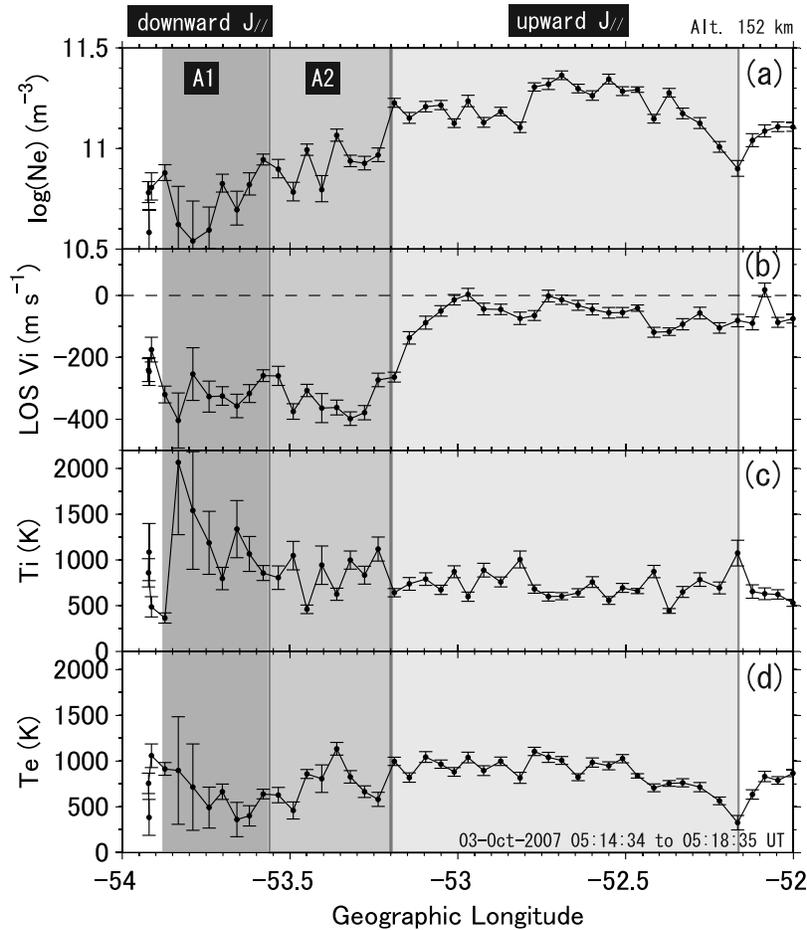
**Figure 5.** (a) Electron density, (b) line-of-sight ion speed, (c) ion temperature, and (d) electron temperature measured with the Sondrestrom IS radar at 152-km altitude. Two areas named as A1 and A2, which are defined in Figure 4, are marked.

neutral wind on the ion-temperature enhancement. In the discussion we ignore heat exchange from electrons to ions. While heat exchange may increase the ion temperature up to a maximum of 200 K above the F2 peak [*St.-Maurice and Hanson*, 1982], the effect should be weaker at 150–200 km. Furthermore, ion-temperature increases appear to be larger than 200 K (see Figure 5).

[20] The *F*-region ion temperature can be explicitly written in the ion-energy equation [*St.-Maurice and Hanson*, 1982; *Oyama et al.*, 2004].

$$T_i = T_n + T_{ie} + \frac{m_i \phi_{in}}{3 k_B \psi_{in}} (V_i - V_n)^2 \qquad (1)$$

where

$$T_{ie} = \frac{(m_i + m_n) \nu_{ie}}{m_i \nu_{in} \psi_{in}} (T_e - T_i) \qquad (2)$$

$$\nu_{ie} = 18.5 \times 10^{-10} \frac{N_e}{T_e^{3/2}} \qquad (3)$$

and

$$\nu_{in} = 3.67 \times 10^{-17} N_n \sqrt{T_{in}} (1 - 0.064 \log_{10} T_{in})^2 \qquad (4)$$

where $T_i$, $T_e$, and $T_n$ are the ion, electron, and neutral temperatures, respectively, $T_{in}$ is equal to $(T_i + T_n)/2$, $m_i$ and $m_n$ are the ion and neutral masses, respectively, $N_n$ and $N_e$ are the number density of neutrals and electrons, respectively, $V_i$ and $V_n$ are the ion and neutral velocities, respectively, $k_B$ is the Boltzmann constant, $\nu_{in}$ and $\nu_{ie}$ are the ion-neutral and ion-electron collision frequencies, respectively [*Schunk and Nagy*, 2000]. Here we assume that $\psi_{in}$ and $\varphi_{in}$, which are the velocity-dependent correction factor [see *Schunk*, 1977, Appendix B] are equal to 1 for all ion-neutral interactions. Ideally all parameters in these equations should be given in the individual areas, A1 and A2. The parameters, which are not given by the IS radar, are $m_i$ and thermospheric parameters, such as $T_n$, $N_n$, $V_n$, and $m_n$. In this calculation $m_i$ is given by a value used for IS-spectrum analysis (27.8 $m_p$ at 152 km height; $m_p$: proton mass) and the thermospheric parameters except for $V_n$ are given by NRLMSIS-00 (Mass Spectrometer Incoherent Scatter) model [*Picone et al.*, 2002]. Further-

**Table 1.** Values Substituted Into Equation (5)[a]

| MSIS | | IS radar | | |
| --- | --- | --- | --- | --- |
| | | | A1 | A2 |
| $T_n$ (K) | 655 | $[N_e]$ (m$^{-3}$) | $4.0 \times 10^{10}$ | $7.9 \times 10^{10}$ |
| [O] (m$^{-3}$) | $1.0 \times 10^{16}$ | $V_i^{LOS}$ (m s$^{-1}$) | 350 | 350 |
| [N$_2$] (m$^{-3}$) | $2.6 \times 10^{16}$ | $T_i$ (K) | 1200 | 800 |
| [O$_2$] (m$^{-3}$) | $3.4 \times 10^{15}$ | $T_e$ (K) | 750 | 750 |

[a]IS radar data were taken from Figure 5, and MSIS data were calculated assuming 152-km height.

more, we assume that these model-dependent parameters do not have horizontal shears in A1 and A2. We also assume that the ion speed parallel to the auroral arc is dominant in A1 and A2 compared to the perpendicular speed. This is a reasonable assumption according to the ionospheric current closure system, which produces the intense electric field perpendicular to the auroral arc. Thus the ion velocity vector in equation (1) can be simply replaced by the LOS ion speed of the IS radar. Therefore only $V_n$, which has three components, is now unknown parameter. $V_n$ cannot be explicitly determined because of only one equation of equation (1); but we can derive difference of the neutral wind speed between A1 and A2 by assuming that only the parallel component to the auroral arc has horizontal shears.

$$\left| V_{n,A2}^{para} - V_{n,A1}^{para} \right| = \left| \sqrt{\frac{3k_B}{m_n} \left( T_{i,A2} - T_n - T_{ie,A2} \right)} - \sqrt{\frac{3k_B}{m_n} \left( T_{i,A1} - T_n - T_{ie,A1} \right)} \right| \qquad (5)$$

Thermospheric and ionospheric values listed in Table 1 are substituted into equation (5), which gives 355 m s$^{-1}$ for the horizontal wind shear. Since IS radar data for this calculation are taken from Figure 5, MSIS data are derived assuming 152 km height same as Figure 5. This means that the wind shear mentioned above is derived for that height. Actually, we have conducted the calculation by using data taken from 140 to 174 km; but there is no significant difference in the results among them. That is reasonable because the thermospheric winds at $F$-region heights generally do not have notable altitude shears [Killeen et al., 1982]. As mentioned above, observed data are not available to confirm whether the estimated wind shear is reasonable for this event. However, the wind magnitude is not surprisingly large compared with previous observations [Greet et al., 1999; Richmond et al., 2003; Griffin et al., 2008] and simulations [Ridley et al., 2003; Deng and Ridley, 2006] though may be larger than the long-term average of quiet-time data [Emmert et al., 2003].

[21] In the previous paragraph, discussion has been focused on relative differences seen in the ion temperature and the ion speed between A1 and A2; but we can find more detailed signatures in the two areas. There are one-to-one correspondences among the electron density, LOS ion speed, and the ion temperature in A1 and A2. Lower electron density coincides with larger LOS ion-speed magnitude and higher ion temperature. While the spatial resolution designed for the experiment with the IS radar may

not be sufficient to study in more quantitative manner, such good correspondence suggests that there are more detailed structures in the ionosphere and the thermosphere around the auroral arc.

[22] On average, the polar ionosphere and thermosphere act as a sink of the energy input from the magnetosphere. A major part of the dissipated energy is transformed into the thermal energy and mechanical energy, although the ratio between the two energies is dependent on the particular ionospheric and thermospheric condition. At the initial moment when the electromagnetic energy has been transferred from the magnetosphere to the ionosphere, the ionosphere at both A1 and A2 must have received equivalent energies. However, the amount of momentum transfer from the plasma to the neutral particles through the collision process could be different between A1 and A2 because of more particle precipitations or higher $F$-region density in A2 than A1. Figure 6 is a diagram that shows how to transform the thermal and mechanical energies between plasmas and neutral particles for this event. The arrow illustrates the direction of individual effects, and the width presents qualitative importance of the effects. Actually, the thermal and mechanical energies are not explicitly separated in the diagram. To do so, we need more quantitative calculations using data of the thermospheric wind, temperature, and density obtained from the observation. However, such data are not available for this event. Larger plasma density in A2 than A1 causes more efficient acceleration of the neutral particles in A2 through the collision process (♦). This suggests that the relative velocity between the neutral wind and the ion velocity is smaller in A2 than A1. The smaller relative velocity reduces the frictional heating rate then suppresses enhancements in the ion temperature. The suppression is thus more significant in A2 than A1 (♥), and the ion temperature measured with the IS radar in A2 is lower than that in A1. The heat transfer from plasmas to neutral particles in A1 may be identical to that in A2, although the ion temperature in A1 is higher than A2 (♣). This is because of a difference in the ion-neutral collision frequency. If so, the neutral temperature should not have obvious horizontal shears to change the horizontal pressure gradient, which is an important parameter for the thermospheric wind dynamics in the $F$ region. Thus we suggest that only possible mechanism to cause the wind shear is the momentum transfer from the accelerated ions by the intense electric field to the neutral particles. To prove this hypothesis, characteristic time to define the thermospheric response to a change in ion motions is the next important issue. The previous studies have suggested that it takes more than 10 min for the momentum transfer from ions to neutrals at $F$-region heights [Baron and Wand, 1983; Killeen et al., 1984; Kosch et al., 2001]. Since the similar horizontal pattern as presented in Figure 4 appeared for at least 16 min, the momentum transfer may work to establish the horizontal wind shear. However, it should be noted that the ion-drag time constant for the momentum transfer was defined neglecting the pressure gradient term in the momentum equation for the neutral gas, although response of the ion temperature may be more prompt (less than a few tens of seconds) [Baron and Wand, 1983]. If the thermal energy transfer from ions to neutrals can also generate the pressure
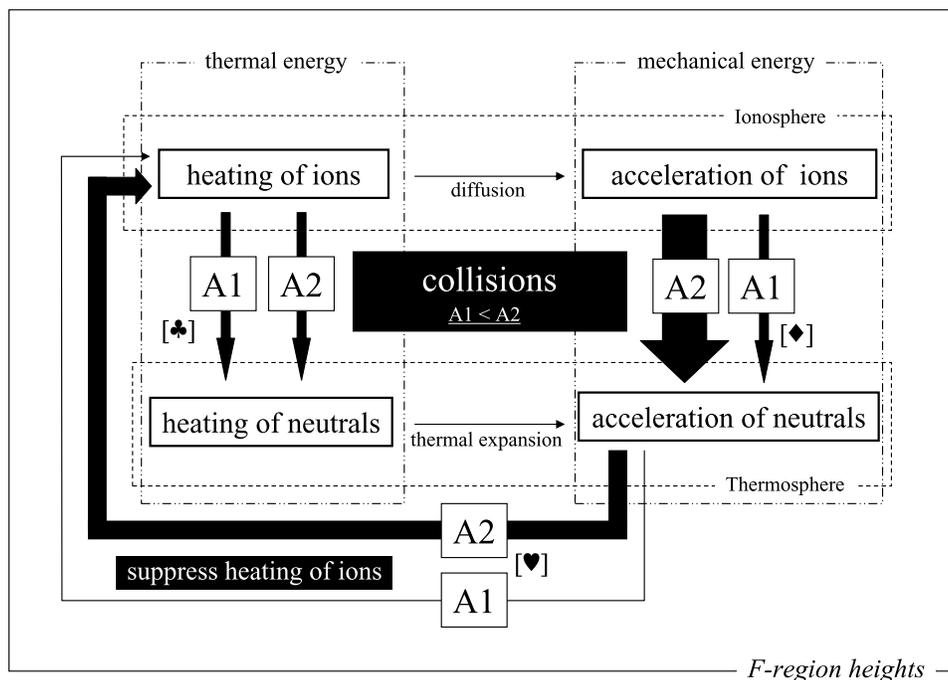
**Figure 6.** Diagram illustrating how to transform the thermal and mechanical energy in the ionosphere and thermosphere for this event. The arrow shows the direction of individual effects, and the width represents the qualitative importance of the effects. A1 and A2 are identical signs used in Figure 4.

gradient in the thermosphere, the characteristic time may be decreased than the ion drag time constant.

## 6. Summary and Conclusions

[23] The simultaneous observations were conducted with the Sondrestrom IS radar and the Reimei satellite on 03 October 2007 around 05:17 UT (02:54 MLT) in order to measure the horizontal pattern of the ionospheric parameters adjacent to the auroral arc. The camera on board the Reimei satellite captured an auroral arc nearly aligned parallel to an L shell. Gross ionospheric features measured with the IS radar around the arc were in fairly good agreement with the previous results from satellite and radar observations. However, the horizontal pattern of the ion temperature was characterized by a localized signature different from the previous results. The ion temperature at the magnetic poleward side of the auroral arc was separated into the two areas, which were almost aligned with the arc of width of ∼10 km: A1 with enhancements in both the ion speed and the ion temperature and A2 with smaller enhancements in the ion temperature but with ion-speed enhancements on the same level with A1. The frictional heating process is a dominant physical mechanism to cause ion-temperature enhancements in the F region. Since the frictional heating rate is a function of the relative speed between ions and neutral particles, the ion-temperature pattern suggested that the neutral wind in A2 was approximately equal to the ion velocity but the neutral wind in A1 had some significant differences from the ion velocity. This revealed that the neutral wind had a horizontal shear within a region with a ∼20 km width, because the ion speed in the two areas was

almost identical. The neutral wind in A2 was considered to be accelerated more efficiently by ion drag than A1 because of higher electron density in A2 because of more particle precipitations.

## References

Andersson, L., R. Ergun, D. Newman, J. McFadden, C. Carlssonm, and Y.-J. Su (2002), Characteristics of parallel electric fields in the downward current region, *Phys. Plasmas*, *9*, 3600–3609.
Aruliah, A. L., and E. M. Griffin (2001), Evidence of meso-scale structure in the high-latitude thermosphere, *Ann. Geophys.*, *19*, 36–46.
Aruliah, A. L., D. Rees, and T. J. Fuller-Rowell (1991a), The combined effect of solar and geomagnetic activity on high latitude thermospheric neutral winds. I: Observations, *J. Atmos. Terr. Phys.*, *53*, 467–483.
Aruliah, A. L., D. Rees, and A. Steen (1991b), Seasonal and solar cycle variations in high-latitude thermospheric winds, *Geophys. Res. Lett.*, *18*(11), 1983–1986.
Aruliah, A. L., E. M. Griffin, A. D. Aylward, E. A. K. Ford, M. J. Kosch, C. J. Davis, V. S. C. Howells, S. E. Pryse, H. R. Middleton, and J. Jussila (2005), First direct evidence of meso-scale variability on ion-

neutral dynamics using co-located tristatic FPIs and EISCAT radar in Northern Scandinavia, *Ann. Geophys.*, *23*, 147–162.

Asamura, K., D. Tsujita, H. Tanaka, Y. Saito, T. Mukai, and M. Hirahara (2003), Auroral particle instrument onboard the INDEX satellite, *Adv. Space Res.*, *32*, 375–378.

Baron, M. J., and R. H. Wand (1983), F region ion temperature enhancements resulting from Joule heating, *J. Geophys. Res.*, *88*(A5), 4114–4118.

Cahill, L. J., R. L. Arnoldy, and W. W. L. Taylor (1980), Rocket observations at the northern edge of the eastward electrojet, *J. Geophys. Res.*, *85*(A7), 3407–3413.

Carlson, C. W., and M. C. Kelley (1977), Observation and interpretation of particle and electric field measurements inside and adjacent to an active auroral arc, *J. Geophys. Res.*, *82*(16), 2349–2360.

Cierpka, K., M. J. Kosch, M. Rietveld, K. Schlegel, and T. Hagfors (2000), Ion-neutral coupling in the high-latitude F-layer from incoherent scatter and Fabry-Perot interferometer measurements, *Ann. Geophys.*, *18*, 1145–1153.

Codrescu, M. V., T. J. Fuller-Rowell, J. C. Foster, J. M. Holt, and S. J. Cariglia (2000), Electric field variability associated with the Millstone Hill electric field model, *J. Geophys. Res.*, *105*(A3), 5265–5273.

Conde, M., J. D. Craven, T. Immel, E. Hoch, H. Stenbaek-Nielsen, T. Hallinan, R. W. Smith, J. Olson, and W. Sun (2001), Assimilated observations of thermospheric winds, the aurora, and ionospheric currents over Alaska, *J. Geophys. Res.*, *106*(A6), 10,493–10,508.

Crickmore, R. I. (1994), Mean thermospheric winds observed from Halley, Antarctica, *Ann. Geophys.*, *12*, 1101–1113.

Davies, J. A., and T. R. Robinson (1997), Heating of the high-latitude ionospheric plasma by electric field, *Adv. Space Res.*, *20*(6), 1125–1128.

de la Beaujardiere, O., and R. Vondrak (1982), Chatanika radar observations of the electrostatic potential distribution of an auroral arc, *J. Geophys. Res.*, *87*(A2), 797–809.

de la Beaujardiere, O., R. Vondrak, and M. Baron (1977), Radar observations of electric fields and currents associated with auroral arcs, *J. Geophys. Res.*, *82*(32), 5051–5062.

de la Beaujardiere, O., R. Vondrak, R. Heelis, W. Hanson, and R. Hoffman (1981), Auroral arc electrodynamic parameters measured by AE-C and the Chatanika radar, *J. Geophys. Res.*, *86*(A6), 4671–4685.

Deng, Y., and A. J. Ridley (2006), Dependence of neutral winds on convection E-field, solar EUV, and auroral particle precipitation at high latitudes, *J. Geophys. Res.*, *111*, A09306, doi:10.1029/2005JA011368.

Emmert, J. T., B. G. Fejer, and D. P. Sipler (2003), Climatology and latitudinal gradients of quiet time thermospheric neutral winds over Millstone Hill from Fabry-Perot interferometer measurements, *J. Geophys. Res.*, *108*(A5), 1196, doi:10.1029/2002JA009765.

Ergun, R. E., et al. (1998), FAST satellite observations of electric field structures in the auroral zone, *Geophys. Res. Lett.*, *25*(12), 2025–2028.

Ergun, R., C. Carlsson, J. McFadden, F. Mozer, and R. Strangeway (2000), Parallel electric fields in discrete arcs, *Geophys. Res. Lett.*, *27*(24), 4053–4056.

Ergun, R., L. Andersson, D. Main, Y.-J. Su, C. Carlsson, J. McFadden, and F. Mozer (2002), Parallel electric fields in the upward current region of the aurora: Indirect and direct observations, *Phys. Plasmas*, *9*, 3685–3694.

Evans, D. S., N. C. Maynard, J. Trøim, T. Jacobsen, and A. Egeland (1977), Auroral vector electric field and particle comparisons: 2. Electrodynamics of an arc, *J. Geophys. Res.*, *82*(16), 2235–2249.

Figueriredo, S., G. Marklund, T. Karlssono, T. Johansson, Y. Ebihara, M. Ejiri, N. Ivchenko, P.-A. Lindqvist, H. Nilsson, and A. Fazakerley (2005), Temporal and spatial evolution of discrete auroral arcs as seen by Cluster, *Ann. Geophys.*, *23*, 2531–2557.

Francis, S. H. (1974), A theory of medium-scale travelling ionospheric disturbances, *J. Geophys. Res.*, *79*(34), 5245–5260.

Freja Special Issue (1998), Freja investigations of high-latitude plasma processes, *J. Geophys. Res.*, *103*(A3), 4119–4375.

Fujii, R., S. Nozawa, N. Matuura, and A. Brekke (1998), Study on neutral wind contribution to the electrodynamics in the polar ionosphere using EISCAT CP-1 data, *J. Geophys. Res.*, *103*(A7), 14,731–14,740.

Fujii, R., S. Nozawa, S. C. Buchert, and A. Brekke (1999), Statistical characteristics of electromagnetic energy transfer between the magnetosphere, the ionosphere, and the thermosphere, *J. Geophys. Res.*, *104*(A2), 2357–2366.

Fujii, R., S. Oyama, S. C. Buchert, S. Nozawa, and N. Matuura (2002), Field-aligned ion motions in the E and F regions, *J. Geophys. Res.*, *107*(A5), 1049, doi:10.1029/2001JA900148.

Fujiwara, H., S. Maeda, H. Fukunishi, T. J. Fuller-Rowell, and D. S. Evans (1996), Global variations of thermospheric winds and temperatures caused by substorm energy injection, *J. Geophys. Res.*, *101*(A1), 225–239.

Fuller-Rowell, T. J., and D. Rees (1980), A three-dimensional time-dependent global model of the thermosphere, *J. Atmos. Sci.*, *37*, 2545–2567.

Fuller-Rowell, T. J. (1984), A two-dimensional, high-resolution, nested-grid model of the thermosphere: 1. Neutral response to an electric field "spike", *J. Geophys. Res.*, *89*(A5), 2971–2990.

Fuller-Rowell, T. J., M. V. Codrescu, H. Rishbeth, R. J. Moffett, and S. Quegan (1996), On the seasonal response of the thermosphere and ionosphere to geomagnetic storms, *J. Geophys. Res.*, *101*(A2), 2343–2353.

Greet, P. A., M. G. Conde, P. L. Dyson, J. L. Innis, A. M. Breed, and D. J. Murphy (1999), Thermospheric wind field over Mawson and Davis, Antarctica, Simultaneous observations by two Fabry-Perot spectrometers of (630 nm emission), *J. Atmos. Sol. Terr. Phys.*, *61*, 1025–1045.

Griffin, E. M., A. L. Aruliah, I. McWhirter, H.-C. I. Yiu, A. Charalambous, and I. McCrea (2008), Upper thermospheric neutral wind and temperature measurements from an extended spatial field, *Ann. Geophys.*, *26*, 2649–2655.

Gustavsson, G., et al. (1997), The electric field and wave experiment for the Cluster mission, *Space Sci. Rev.*, *79*(1–2), 137–156, doi:10.1023/A:1004975108657.

Hajkowicz, L. A. (1991), Auroral electrojet effect on the global occurrence pattern of large scale travelling ionospheric disturbances, *Planet. Space Sci.*, *39*, 1189–1196.

Hocke, K., and K. Schlegel (1996), A review of atmospheric gravity waves and travelling ionospheric disturbances: 1982–1995, *Ann. Geophys.*, *14*, 917–940.

Hultqvist, B. (2002), Downward ion acceleration at auroral latitudes: Cause of parallel electric field, *Ann. Geophys.*, *20*, 1117–1136.

Hunsucker, R. D. (1982), Atmospheric gravity waves generated in the high-latitude ionosphere: A review, *Rev. Geophys.*, *20*(2), 293–315.

Hwang, K.-J., K. A. Lynch, C. W. Carlson, J. W. Bonnell, and W. J. Peria (2006a), Fast Auroral Snapshot observations of perpendicular DC electric field structures in downward auroral current regions: Morphology, *J. Geophys. Res.*, *111*, A09205, doi:10.1029/2005JA011471.

Hwang, K.-J., K. A. Lynch, C. W. Carlson, J. W. Bonnell, and W. J. Peria (2006b), Fast Auroral Snapshot observations of perpendicular DC electric field structures in downward current regions: Implications, *J. Geophys. Res.*, *111*, A09206, doi:10.1029/2005JA011472.

Ishii, M., M. Conde, R. W. Smith, M. Krynicki, E. Sagawa, and S. Watari (2001), Vertical wind observations with two Fabry-Perot interferometers at Poker Flat, Alaska, *J. Geophys. Res.*, *106*(A6), 10,537–10,551.

Ishii, M., M. Kubota, M. Conde, R. W. Smith, and M. Krynicki (2004), Vertical wind distribution in the polar thermosphere during Horizontal E Region Experiment (HEX) campaign, *J. Geophys. Res.*, *109*, A12311, doi:10.1029/2004JA010657.

Johansson, T., S. Figueiredo, T. Karlsson, G. Marklund, A. Fazakerley, S. Buchert, P.-A. Lindqvist, and H. Nilsson (2004), Intense high-altitude auroral electric fields: Temporal and spatial characteristics, *Ann. Geophys.*, *22*, 2485–2495.

Johansson, T., G. Marklund, T. Karlsson, S. Liléo, P.-A. Lindqvist, H. Nilsson, and S. Buchert (2007), Scale sizes of intense auroral electric fields observed by Cluster, *Ann. Geophys.*, *25*, 2413–2425.

Karlsson, T., and G. T. Marklund (1996), A statistical study of intense low-altitude electric fields observed by Freja, *Geophys. Res. Lett.*, *23*(9), 1005–1008.

Karlsson, T., and G. Marklund (1998), Simulations of effects of small-scale auroral current closure in the return current region, *Phys. Space Plasmas*, *15*, 401–406.

Kato, S., T. Kawakami, and D. St. John (1977), Theory of gravity wave emission from moving sources in the upper atmosphere, *J. Atmos. Terr. Phys.*, *39*, 581–588.

Killeen, T. L., and R. G. Roble (1988), Thermosphere dynamics: Contributions from the first 5 years of the Dynamics Explorer Program, *Rev. Geophys.*, *26*(2), 329–367.

Killeen, T. L., P. B. Hays, N. W. Spencer, and L. E. Wharton (1982), Neutral winds in the polar thermosphere as measured from Dynamics Explorer, *Geophys. Res. Lett.*, *9*(9), 957–960.

Killeen, T. L., P. B. Hays, G. R. Carignan, R. A. Heelis, W. B. Hanson, N. W. Spencer, and L. H. Brace (1984), Ion-neutral coupling in the high-latitude F region: Evaluation of ion heating terms from Dynamics Explorer 2, *J. Geophys. Res.*, *89*(A9), 7495–7508.

Kintner, P. M., L. J. Cahill Jr., and R. L. Arnoldy (1974), Current system in an auroral substorm, *J. Geophys. Res.*, *79*(28), 4326–4330.

Knudsen, D. J., E. F. Donovan, L. L. Cogger, B. Jackel, and W. D. Shaw (2001), Width and structure of mesoscale optical auroral arcs, *Geophys. Res. Lett.*, *28*(4), 705–708.

Kosch, M. J., K. Cierpka, M. T. Rietveld, T. Hagfors, and K. Schlegel (2001), High-latitude ground-based observations of the thermospheric ion-drag time constant, *Geophys. Res. Lett.*, *28*(7), 1395–1398.

Lynch, K. A., J. W. Bonnell, C. W. Carlson, and W. Peria (2002), Return current region aurora: E-parallel, j(z), particle energization, and broad-

band ELF wave activity, *J. Geophys. Res.*, *107*(A7), 1115, doi:10.1029/2001JA900134.

Lu, G., A. D. Richmond, B. A. Emery, and R. G. Roble (1995), Magnetosphere-ionosphere-thermosphere coupling: Effect of neutral winds on energy transfer and field-aligned current, *J. Geophys. Res.*, *100*(A10), 19,643–19,659.

Maggs, J. E., and T. N. Davis (1968), Measurements of the thickness of auroral structures, *Planet. Space Sci.*, *216*, 205–209, doi:10.1016/0032-0633(68)90069-X.

Marklund, G., I. Sandahl, and H. Opgenoorth (1982), A study of the dynamics of a discrete auroral arc, *Planet. Space Sci.*, *30*(2), 179–197.

Marklund, G., W. Baumjohann, and I. Sandahl (1983), Rocket and ground-based study of an auroral breakup event, *Planet. Space Sci.*, *31*, 207.

Marklund, G. T., L. G. Blomberg, C.-G. Fälthammar, and P.-A. Lindqvist (1994), On intense diverging electric fields associated with black aurora, *Geophys. Res. Lett.*, *21*(17), 1859–1862.

Marklund, G. T., T. Karlsson, and J. Clemmons (1997), On low-altitude particle acceleration and intense electric fields and their relation to black aurora, *J. Geophys. Res.*, *102*(A8), 17,509–17,522.

Marklund, G. T., et al. (2001), Temporal evolution of the electric field accelerating electrons away from the auroral ionosphere, *Nature*, *414*, 724–727, doi:10.1038/41472a.

Marklund, G. T., T. Karlsson, S. Figueiredo, T. Johansson, P.-A. Lindqvist, M. André, S. Buchert, L. Kistler, and A. Fazakerley (2004), Characteristics of quasi-static potential structures observed in the auroral return current region by Cluster, *Nonlinear Proccess. Geophys.*, *11*, 709–716.

Marklund, G. T., T. Johansson, S. Liléo, and T. Karlsson (2007), Cluster observations of an auroral potential and associated field-aligned current reconfiguration during thinning of the plasma sheet boundary layer, *J. Geophys. Res.*, *112*, A01208, doi:10.1029/2006JA011804.

Matsuo, T., A. D. Richmond, and D. W. Nychka (2002), Modes of high-latitude electric field variability derived from DE-2 measurements: Empirical Orthogonal Function (EOF) analysis, *Geophys. Res. Lett.*, *29*(7), 1107, doi:10.1029/2001GL014077.

Matsuo, T., A. D. Richmond, and K. Hensel (2003), High-latitude ionospheric electric field variability and electric potential derived from DE-2 plasma drift measurements: Dependence on IMF and dipole tilt, *J. Geophys. Res.*, *108*(A1), 1005, doi:10.1029/2002JA009429.

Matsuo, T., A. D. Richmond, and G. Lu (2005), Optimal interpolation analysis of high-latitude ionospheric electrodynamics using empirical orthogonal functions: Estimation of dominant modes of variability and temporal scales of large-scale electric fields, *J. Geophys. Res.*, *110*, A06301, doi:10.1029/2004JA010531.

Matsuo, T., and A. D. Richmond (2008), Effects of high-latitude ionospheric electric field variability on global thermospheric Joule heating and mechanical energy transfer rate, *J. Geophys. Res.*, *113*, A07309, doi:10.1029/2007JA012993.

Milan, S. E., and M. Lester (2001), A classification of spectral populations observed in HF radar backscatter from the E-region electrojets, *Ann. Geophys.*, *19*, 189–204.

Milan, S. E., M. Lester, N. Sato, and H. Takizawa (2001), On the altitude dependence of the spectral characteristics of decameter-wavelength E-region backscatter and the relationship with optical auroral forms, *Ann. Geophys.*, *19*, 205–217.

Milan, S. E., N. Sato, M. Lester, T. K. Yeman, Y. Murata, H. Doi, and T. Saemundsson (2002), The spectral characteristics of E-region radar echoes co-located with and adjacent to visual auroral arcs, *Ann. Geophys.*, *20*, 795–805.

Milan, S. E., M. Lester, and N. Sato (2003), Multi-frequency observations of E-region HF radar aurora, *Ann. Geophys.*, *21*, 761–777.

Millward, G. H., S. Quegan, R. J. Moffett, T. J. Fuller-Rowell, and D. Rees (1993), A modeling study of the coupled ionospheric and thermospheric response to an enhanced high-latitude electric field event, *Planet. Space Sci.*, *41*, 45–56.

Moen, J., Y. Rinne, H. C. Carlson, K. Oksavik, R. Fujii, and H. Opgenoorth (2008), On the relationship between thin Birkeland current arcs and reversed flow channels in the winter cusp/cleft ionosphere, *J. Geophys. Res.*, *113*, A09220, doi:10.1029/2008JA013061.

Mozer, F. S., and C. A. Kletzing (1998), Direct observation of large, quasi-static, parallel electric fields in the auroral acceleration region, *Geophys. Res. Lett.*, *25*(10), 1629–1632.

Niciejewski, R. J., T. L. Killeen, and S. C. Solomon (1996), Observations of thermospheric horizontal neutral winds at Watson Lake, Yukon Territory ($\Lambda = 65°$N), *J. Geophys. Res.*, *101*(A1), 241–259.

Oyama, S., M. Ishii, Y. Murayama, H. Shinagawa, S. C. Buchert, R. Fujii, and W. Kofman (2001), Generation of atmospheric gravity waves associated with auroral activity in the polar *F* region, *J. Geophys. Res.*, *106*(A9), 18,543–18,554.

Oyama, S., C. Lathuillere, S. Maeda, and B. J. Watkins (2004), Summer-winter dependencies of day-night differences in the ion temperature in the polar upper *F* region, *Geophys. Res. Lett.*, *31*, L05806, doi:10.1029/2003GL018820.

Oyama, S., B. J. Watkins, S. Maeda, H. Shinagawa, S. Nozawa, Y. Ogawa, A. Brekke, C. Lathuillere, and W. Kofman (2008), Generation of the lower-thermospheric vertical wind estimated with the EISCAT KST radar at high latitudes during periods of moderate geomagnetic disturbance, *Ann. Geophys.*, *26*, 1491–1505.

Picone, J. M., A. E. Hedin, D. P. Drob, and A. C. Aikin (2002), NRLMSISE-00 empirical model of the atmosphere: Statistical comparisons and scientific issues, *J. Geophys. Res.*, *107*(A12), 1468, doi:10.1029/2002JA009430.

Potter, W. E. (1970), Rocket measurements of auroral electric and magnetic fields, *J. Geophys. Res.*, *75*(28), 5415–5431.

Richards, P. G., and P. J. Wilkinson (1998), The ionosphere and thermosphere at southern midlatitudes during the November 1993 ionospheric storm: A comparison of measurement and modeling, *J. Geophys. Res.*, *103*(A5), 9373–9389.

Richmond, A. D., C. Lathuillère, and S. Vennerstroem (2003), Winds in the high-latitude lower thermosphere: Dependence on the interplanetary magnetic field, *J. Geophys. Res.*, *108*(A2), 1066, doi:10.1029/2002JA009493.

Ridley, A. J., A. D. Richmond, T. I. Gombosi, D. L. De Zeeuw, and C. R. Clauer (2003), Ionospheric control of the magnetospheric configuration: Thermospheric neutral winds, *J. Geophys. Res.*, *108*(A8), 1328, doi:10.1029/2002JA009464.

Ruohoniemi, J. M., and R. A. Greenwald (2005), Dependencies of high-latitude plasma convection: Consideration of interplanetary magnetic field, seasonal, and universal time factors in statistical patterns, *J. Geophys. Res.*, *110*, A09204, doi:10.1029/2004JA010815.

Saito, H., et al. (2001), INDEX: Piggy-back satellite for aurora observation and technology demonstration, *Acta Astronaut.*, *48*(5–12), 723–735.

Saito, S., S. C. Buchert, S. Nozawa, and R. Fujii (2001), Observation of isotropic electron temperature in the turbulent E region, *Ann. Geophys.*, *19*, 11–15.

Sakanoi, T., S. Okano, Y. Obuchi, T. Kobayashi, M. Ejiri, K. Asamura, and M. Hirahara (2003), Development of the multi-spectral auroral camera onboard the INDEX satellite, *Adv. Space Res.*, *32*, 379–384.

Schlegel, K., and J. P. St.-Maurice (1981), Anomalous heating of the polar E region by unstable plasma waves: 1. Observations, *J. Geophys. Res.*, *86*(A3), 1447–1452.

Schunk, R. W. (1977), Mathematical structure of transport equations for multispecies flows, *Rev. Geophys.*, *15*(4), 429–445.

Schunk, R. W., and A. F. Nagy (2000), *Ionospheres: Physics, Plasma Physics, and Chemistry*, Cambridge Univ. Press, New York.

Shepherd, S. G., J. M. Ruohoniemi, and R. A. Greenwald (2003), Direct measurements of the ionospheric convection variability near the cusp/throat, *Geophys. Res. Lett.*, *30*(21), 2109, doi:10.1029/2003GL017668.

Sica, R. J., M. H. Rees, G. J. Romick, G. Hernandez, and R. G. Roble (1986), Auroral zone thermospheric dynamics: 1. Averages, *J. Geophys. Res.*, *91*(A3), 3231–3244.

Smith, R. W. (2000), The global-scale effect of small-scale thermospheric disturbances, *J. Atmos. Sol. Terr. Phys.*, *62*, 1623–1628.

Stiles, G. S., J. C. Foster, and J. R. Doupnik (1980), Prolonged radar observations of an auroral arc, *J. Geophys. Res.*, *85*(A3), 1223–1234.

St.-Maurice, J. P., and W. B. Hanson (1982), Ion frictional heating at high latitudes and its possible use for an in situ determination of neutral thermospheric winds and temperature, *J. Geophys. Res.*, *87*(A9), 7580–7602.

Thayer, J. P. (1998), Height-resolved Joule heating rates in the high-latitude E region and the influence of neutral winds, *J. Geophys. Res.*, *103*(A1), 471–487.

Thayer, J. P. (2000), High-latitude currents and their energy exchange with the ionosphere-thermosphere system, *J. Geophys. Res.*, *105*(A10), 23,015–23,024.

Theile, B., R. Boström, A. Dumbs, K. U. Grossman, D. Krankowsky, P. Lämmerzahl, G. Marklund, E. Neske, G. Schmidtke, and K. Wilhelm (1981), in situ measurements of heating parameters in the auroral ionosphere, *Planet. Space Sci.*, *29*, 455–468.

Tsugawa, T., A. Saito, Y. Otsuka, and M. Yamamoto (2003), Damping of large-scale traveling ionospheric disturbances detected with GPS networks during the geomagnetic storm, *J. Geophys. Res.*, *108*(A3), 1127, doi:10.1029/2002JA009433.

Tsugawa, T., A. Saito, and Y. Otsuka (2004), A statistical study of large-scale traveling ionospheric disturbances using the GPS network in Japan, *J. Geophys. Res.*, *109*, A06302, doi:10.1029/2003JA010302.

Villain, J.-P., R. A. Greenwald, K. B. Baker, and J. M. Ruohoniemi (1987), HF radar observations of E-region plasma irregularities produced by oblique electron streaming, *J. Geophys. Res.*, *92*(A11), 12,327–12,342.

Villain, J.-P., C. Hanuise, R. A. Greenwald, K. B. Baker, and J. M. Ruohoniemi (1990), Obliquely propagating ion acoustic waves in the

auroral E-region: Further evidence of irregularity production by field-aligned electron streaming, *J. Geophys. Res.*, *95*(A6), 7833–7846.

Weimer, D. R., C. K. Goertz, D. A. Gurnett, N. C. Maynard, and J. L. Burch (1985), Auroral zone electric fields from DE 1 and 2 at magnetic conjunctions, *J. Geophys. Res.*, *90*(A8), 7479–7494.

Ziesolleck, Ch., W. Baumjohann, K. Brüning, C. W. Carlson, and R. I. Bush (1983), Comparison of height-integrated current densities derived from ground-based magnetometer and rocket-borne observations during the Porcupine F3 and F4 flights, *J. Geophys. Res.*, *88*(A10), 8063–8072.

———————————

K. Asamura and A. Yamazaki, Department of Space Plasma Physics, Japan Aerospace Exploration Agency, Institute of Space and Astronautical Science, 3-1-1 Yoshinodai, Sagamihara, Kanagawa 229-8510, Japan.

R. Fujii, S. Nozawa, S. Oyama, and T. T. Tsuda, Solar-Terrestrial Environment Laboratory, Nagoya University, NULL F3-3 (250), Furo Chikusa, Nagoya, Aichi 464-8601, Japan. (soyama@stelab.nagoya-u.ac.jp)

M. Hirahara, Department of Earth and Planetary Science, Graduate School of Science, University of Tokyo, 7-3-1 Hongo Bunkyo, Tokyo 113-0033, Japan.

Y. Kasaba, Planetary Atmosphere Physics Laboratory, Graduate School of Science, Tohoku University, 6-3 Aoba Aramaki, Sendai, Miyagi 980-8578, Japan.

Y. Obuchi, Genesia Corporation, 601 Mitaka-Sangyo Plaza, 3-38-4 Shimo-Renjyu, Mitaka, Tokyo 181-0013, Japan.

T. Sakanoi, Planetary Plasma and Atmospheric Research Center, Graduate School of Science, Tohoku University, 6-3 Aoba Aramaki, Sendai, Miyagi 980-8578, Japan.

B. J. Watkins, Space Physics and Aeronomy Group, Geophysical Institute, University of Alaska Fairbanks, 903 Koyukuk Drive, P.O. Box 757320, Fairbanks, AK 99775-7320, USA.